Electronic structure and x-ray magnetic circular dichroism in uranium compounds. III. Heavy-fermion compounds

A. N. Yaresko
Max Planck Institute for Physics of Complex Systems, D-01187 Dresden, Germany

V. N. Antonov* and B. N. Harmon
Ames Laboratory, Iowa State University, Ames, Iowa 50011, USA

(Received 10 September 2003; published 24 December 2003)

The electronic structure and x-ray magnetic circular dichroism (XMCD) spectra of heavy-fermion compounds UPt_3, URu_2Si_2, UPd_2Al_3, UNi_2Al_3, and UBe_{13} are investigated theoretically from first principles, using the fully relativistic Dirac linear muffin-tin orbital band-structure method. The electronic structure is obtained with the local spin-density approximation (LSDA), as well as with a generalization of the LSDA $+U$ method. The origin of the XMCD spectra in the compound is examined.

DOI: 10.1103/PhysRevB.68.214426 PACS number(s): 75.30.Mb, 71.28.+d

I. INTRODUCTION

One of the most fascinating aspects of heavy-fermion physics is the observation of superconductivity, first detected in $CeCu_2Si_2$ by Steglich *et al.*[1] This is a milestone in the field of superconducting materials, along with the discoveries of superconductivity in the cuprate compounds and in fullerenes.

Heavy-fermion materials have been at the forefront of condensed-matter research because the strongly correlated electronic states responsible for their physical properties remain a very challenging problem. These materials display exotic behavior in their thermodynamic and transport properties at moderate temperatures, and many heavy-fermion materials have unusual coexisting states at low temperatures.[2–8] A fascinating aspect of this class of compounds is the wealth of ground states which occur. Although a myriad of experiments have been devoted to the characterization of these ground states, a comprehensive understanding of heavy-fermion properties at low temperature is still lacking. The heavy-fermion ground-state properties are highly sensitive to impurities, chemical composition, and slight changes of external parameters. This sensitivity indicates that a subtle interplay between different interactions produces a richness of experimental phenomena. It is widely believed that the competition between the Kondo effect (reflecting the interaction between the localized $5f$ moments and the conduction electrons) and the magnetic correlations between the periodically arranged $5f$ moments constitute the key factors in determining the magnetic properties of heavy-fermion compounds.[2]

For heavy-fermion compounds the attribute ''heavy'' is connected with the observation of a characteristic energy much smaller than in ordinary metals, which reflects a thermal effective mass m^* of the conduction electrons orders of magnitude larger than the bare electron mass. These heavy masses manifest themselves by a large electronic coefficient γ of the specific heat C ($\gamma = C/T$ for $T \rightarrow 0$), an enhanced Pauli susceptibility, a huge T^2 term in the electrical resistivity, and highly temperature-dependent de Haas–van Alphen oscillation amplitudes at very low temperatures. The large m^* value is usually believed to be derived from strongly correlated electrons. While at high temperature the $5f$ electrons and conduction electrons interact weakly, at low temperature these two subsets of electrons become strongly coupled, resulting in the formation of a narrow resonance manifested in the density of states near the Fermi energy. Thus, at sufficiently low temperatures, the heavy-fermion compounds behave like a system of heavy itinerant electrons, the properties of which can be described in the framework of the Landau Fermi-liquid formalism.

Among uranium heavy-fermion compounds superconductivity is observed in UBe_{13}, UPt_3, URu_2Si_2, U_2PtC_2, UPd_2Al_3, and UNi_2Al_3. Usually superconductivity in these compounds coexists with antiferromagnetic order, and this has led to the suggestion that the effective attractive interaction between the superconducting electrons may be mediated by spin fluctuations, rather than by the electron-phonon interaction. This is supported by the fact that the observed superconducting states are highly anisotropic, with nodes in the gap function not explainable by an *s*-wave theory.

In recent years, it has been shown that polarized x rays can be used to determine the magnetic structure of magnetically ordered materials by x-ray scattering and x-ray magnetic circular dichroism (XMCD). Nowadays, the investigation of magneto-optical effects in the soft x-ray range has gained great importance as a tool for the investigation of magnetic materials. Recently, XMCD measurements have been successfully performed on some uranium heavy-fermion compounds such as UBe_{13} and UPt_3,[9] UNi_2Al_3,[10] UPd_2Al_3, and URu_2Si_2.[11]

In the present work we report a detailed theoretical investigation of the electronic structure and XMCD properties of heavy-fermion uranium compounds UPt_3, URu_2Si_2, UPd_2Al_3, UNi_2Al_3, and UBe_{13}. This paper is the last in a series of three papers. The first paper[12] is devoted to theoretical investigation of the XMCD spectra of UFe_2 and the second one to XMCD properties of U*X*Al (*X*=Co, Rh, and Pt) intermetallics.[13] The degree of localization of U $5f$ states and, hence, the strength of the Coulomb f-f correlation ef-

 ©2003 The American Physical Society

fects increases from UFe_2 to UXAl and to heavy-fermion compounds.

This paper is organized as follows. Section II presents a description of the computational details. Sections III–VI are devoted to the electronic structure and XMCD properties of the UPt_3, URu_2Si_2, UX_2Al_3 (X=Pd and Ni), and UBe_{13}, respectively, calculated in the local spin-density approximation (LSDA) and LSDA+U. The XMCD theoretical calculations are compared to the experimental measurements. Finally, the results are summarized in Sec. VII.

II. COMPUTATIONAL DETAILS

The details of the computational method are described in the first paper of this series,[12] and here we only mention several aspects. The calculations were performed using the linear muffin-tin orbital (LMTO) method[14,15] in the atomic sphere approximation with the combined correction term taken into account. We used the von Barth-Hedin parametrization[16] for the exchange-correlation potential. Brillouin-zone integrations were performed using the improved tetrahedron method,[17] and self-consistency charge was obtained with 301, 1183, 910, and 349 irreducible **k** points for UPt_3, URu_2Si_2, UPd_2Al_3, and UBe_{13}, respectively. The basis consisted of U *s*, *p*, *d*, *f*; transition metal (Pt, Ru, Pd, and Ni) *s*, *p*, and *d*; Si, Al, and Be *s* and *p* LMTO's. The electronic structure is obtained with the LSDA, as well as with a generalization of the LSDA+U method for which the occupation matrix of localized electrons becomes nondiagonal in spin indices in the presence of spin-orbit (SO) coupling.[18]

III. UPt_3

UPt_3 is a well-known heavy-fermion system.[19,20] The Sommerfeld coefficient of the linear low-temperature specific heat is strongly enhanced, i.e., $\gamma=420$ mJ/(mol K^2). Strong electron-electron correlations are also manifest in a $T^3 \ln T$ term in the low-temperature specific heat, which is believed to be due to spin fluctuations. At low temperature UPt_3 is a superconductor, with a T_c of 0.54 K.[7] UPt_3 is the archetype of a heavy-fermion system. It has the qualitative properties of a Fermi liquid, but the magnitude of the effective masses, reflected in the specific heat and magnetic susceptibility, is very much larger than the free-electron value. The heaviness of the electrons is generally attributed to electron correlations which come from the strong Coulomb interactions among the localized $5f$ electrons on the U sites.

UPt_3 has attracted a great deal of interest from band-structure theorists,[21–25] particularly when it became clear that reliable experimental information on the Fermi surface could be obtained by measurements of the de Haas–van Alphen (dHvA) effect.[26–28] These experiments unambiguously confirm that UPt_3 has to be regarded as a strongly correlated Fermi liquid. Although a detailed picture of the low-temperature phase of UPt_3 has emerged, a comprehensive theoretical picture of the heavy quasiparticles is still missing.

It has been considered a success of the LSDA that the dHvA frequencies could be related to extremal orbits on the Fermi surface obtained from band-structure calculations which treat the U $5f$ states as itinerant. There are good reasons that standard band-structure calculations reproduce well the complex topology of the Fermi surface in UPt_3. In great contrast, however, no such agreement is found for the measured cyclotron masses. The calculated energy bands are too broad to explain the effective masses: dHvA masses are by a factor of order 20 bigger than the band masses m_b obtained from the LSDA calculations.[23–25] This is of course the defining characteristic of a heavy-fermion compound, and is due to the strong electron-electron correlations not included in the band-structure calculations. It is interesting that even in the presence of such strong correlations, there is no evidence of any breakdown of the Fermi-liquid theory. The standard Lifshitz-Kosevich formula for the field and temperature dependence of the amplitude of quantum oscillations is perfectly verified down to 10 mK and up to 18 T.[7]

UPt_3 shows a static antiferromagnetic order below about $T_N=5$ K with a very small staggered moment of the order of 0.01 μ_B/U atom. This ordering was first noticed in muon-spin-relaxation measurements by Heffner *et al.*[29] and was soon confirmed by neutron scattering.[30] The magnetic order is collinear and commensurate with the crystal lattice, with a moment aligned in the basal plane. It corresponds to antiferromagnetic coupling within planes and ferromagnetic coupling between planes. All aspects of this ordering were reproduced by later neutron studies on a different crystal[31,32] and by magnetic x-ray scattering.[33] The moment at lower temperatures grows to a maximum magnitude of $(0.02–0.03)\mu_B$/U atom.

A. Band structure

UPt_3 crystallizes in the $MgCd_3$-type structure. The uranium atoms form a closed-packed hexagonal structure with the platinum atoms bisecting the planar bonds. There are two formula units per unit cell. The compound belongs to the space group $P6_3/mmc$ and the point group D_{6h}. The lattice parameters are $a=5.753$ Å and $c/a=4.898$. The nearest U-U distance is between atoms in adjacent layers, equal to 4.132 Å, and the conductivity is greatest along the c axis.

The fully relativistic spin-polarized LSDA energy band structure and total density of states (DOS) of the ferromagnetic UPt_3 compound is shown in Fig. 1. The occupied part of the valence band is formed predominantly by Pt $5d$ states. The characteristic feature of the LSDA band structure is a narrow peak of U $5f_{5/2}$ states situated just at the Fermi level (E_F) 1.0 eV above the top of Pt $5d$ states. U $5f_{7/2}$ states are split off by strong SO coupling and form another narrow peak 1 eV above E_F.

Figure 1 also shows the band structure of UPt_3 calculated in the LSDA+U approximation with $U=2.0$ eV and $J=0.5$ eV. The Coulomb repulsion splits partially occupied U $5f_{5/2}$ states and the LSDA+U calculations give a solution with two localized $5f$ electrons. These localized $5f$ states are situated above the top of Pt $5d$ and form a rather narrow peak at 0.2 eV below E_F. The position of the peak agrees well with the results of recent resonant photoemission

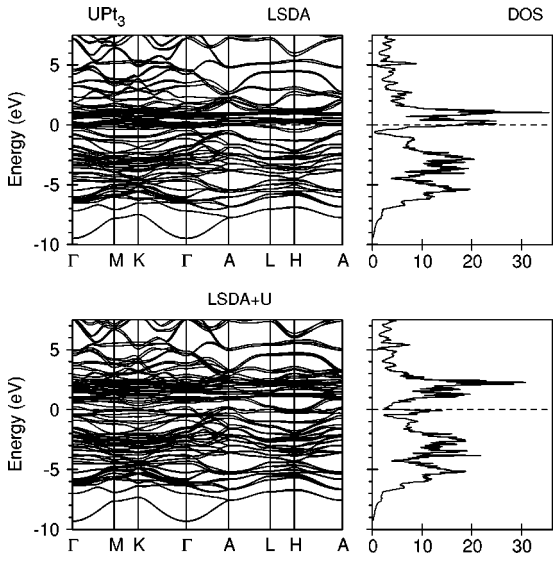

FIG. 1. The self-consistent fully relativistic, spin-polarized energy band structure and total DOS [in states/(unit cell eV)] of UPt_3 calculated in the LSDA and LSDA+U.

spectroscopy[34] (PES) and angle-resolved PES measurements.[35] U $5f$ states just above the Fermi level are formed by the remaining $5f_{5/2}$ states whereas the peak from the $5f_{7/2}$ states is pushed from its LSDA position at 1 eV above E_F to 2.3 eV.

An orbital resolved DOS corresponding to the orbitals with the largest occupation numbers is shown in Fig. 2 for UPt_3 and for UPd_3 as a reference material. Two peaks at -1.0 to -0.5 eV in UPd_3 are formed by $5f_{5/2}$ states with $m_j=-5/2$ and $m_j=-3/2$. Their occupation numbers are $n_{5/2}=0.988$ and $n_{3/2}=0.982$, which corresponds to an f^2 configuration of the U ion.[18] The corresponding states in UPt_3 are situated in -0.5 to 0.2 eV energy range, very close to the Fermi level and partially occupied. Such a different energy position of occupied $5f_{5/2}$ states in UPd_3 and UPt_3 can be explained by the larger spatial extent of Pt $5d$ wave functions as compared to the Pd $4d$ states, which causes a

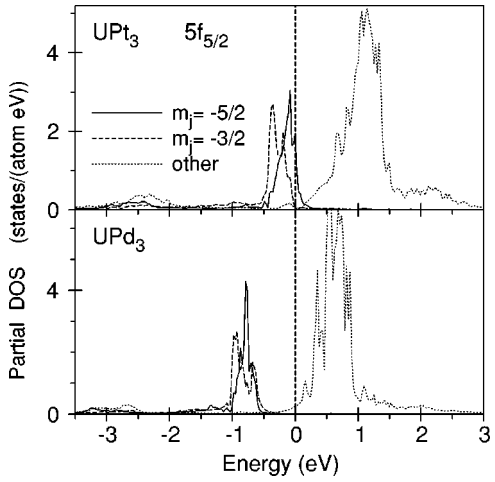

FIG. 2. The partial $5f_{5/2}$ density of states (in states/atom eV) in UPt_3 and UPd_3 calculated in the LSDA+U.

proportional increase of the part of f electron density at the U site provided by the ''tails'' of d states. The screening of the localized U $5f$ states by this delocalized density becomes stronger in UPt_3 and their occupied $5f_{5/2}$ states shift to higher energy.[18]

The above-mentioned self-consistent LSDA+U solutions for UPd_3 and UPt_3 are magnetic with a rather large U magnetic moment. This is contrary to the experimental data which show that the ordered magnetic moment is only 0.01 μ_B and (0.02–0.03) μ_B per U atom in UPd_3 and UPt_3, respectively.[31–33,36] This extremely small U magnetic moment is explained by the fact that according to the crystalline electric-field (CEF) level scheme derived from neutron-scattering experiments, the lowest CEF level of U^{4+} ion in both compounds is a singlet[33,37] which leads to a nonmagnetic ground state for these compounds. The LSDA+U is still a one-electron approximation and cannot fully account for the subtle many-body effects responsible for the small value of the U magnetic moment in UPd_3 and UPt_3. It tries to obey Hund's rules in the only way it is allowed to, i.e., by producing a magnetic solution. A possible way to overcome this discrepancy between the calculations and the experiment is to force a nonmagnetic ground state in the LSDA+U calculations as it was done by Harima and co-workers in Refs. 38 and 36. We have verified, however, that this leads to an increase of the total energy as compared to magnetic states obtained in the calculations.

It should be mentioned that depending on the starting conditions another self-consistent LSDA+U solution very close in total energy can be obtained for UPd_3 as well as for UPt_3. This solution also results in two localized U $5f$ electrons but in this case the occupied states are $|\frac{5}{2},-\frac{5}{2}\rangle$ and $|\frac{5}{2},-\frac{1}{2}\rangle$ (here we used the notation $|j,m_j\rangle$ for the state with the total momentum j and its projection m_j). The existence of two almost degenerate solutions can be understood if one compares the matrix elements of Coulomb interaction $U_{m_j,m_j'}$ calculated between $5f_{5/2}$ states with different m_j.[18] The matrix elements $U_{5/2,3/2}$ and $U_{5/2,1/2}$ are equal and the energy difference is caused not by the on-site Coulomb interaction but instead by a difference in the hybridization between U $5f_{5/2}$ and conduction electrons. Also, the lowest unoccupied $5f$ state, which is either $|\frac{5}{2},-\frac{1}{2}\rangle$ or $|\frac{5}{2},-\frac{3}{2}\rangle$, feels the same Coulomb repulsion of the localized electrons. Total-energy calculations, however, show that lower-energy solution is associated with $|\frac{5}{2},-\frac{3}{2}\rangle$ occupied states.

B. XMCD spectra

As we mentioned above, for the $5f^2$ configuration in UPt_3 we have two solutions with close total energies, in the first case the $5f_{5/2}$ states with $m_j=-5/2$ and $-3/2$ are occupied and in the second case the occupied states are $m_j=-5/2$ and $-1/2$. In the first case the dipole allowed transitions for left circularly polarized light $\lambda=+1$ are $-3/2\rightarrow-1/2$, $-1/2\rightarrow+1/2$, $+1/2\rightarrow+3/2$, and $+3/2\rightarrow+5/2$ and for right circularly polarization $\lambda=-1$ are $+1/2\rightarrow-1/2$ and $+3/2\rightarrow+1/2$. The transitions with equal final states $m_j=-1/2$ and $m_j=+1/2$ mostly cancel each other and the XMCD

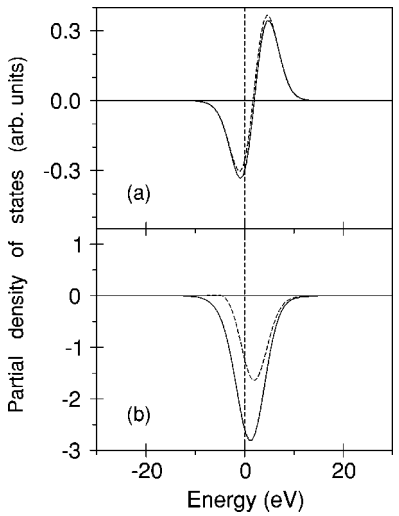

FIG. 3. The model representation of the M_5 (a) and M_4 (b) XMCD of UPt_3 for two solutions with $|\frac{5}{2},-\frac{3}{2}\rangle$ occupied states (full lines) and $|\frac{5}{2},-\frac{1}{2}\rangle$ ones (dashed lines): (a) presents the partial densities of states $[N^{7/2}_{-7/2}+N^{7/2}_{-5/2}]-[N^{7/2}_{7/2}+N^{7/2}_{5/2}]$; (b) $-[N^{5/2}_{3/2}+N^{5/2}_{5/2}]$ (full line) and $N^{5/2}_{1/2}-[N^{5/2}_{3/2}+N^{5/2}_{5/2}]$ (dashed lines) (see the explanation in the text).

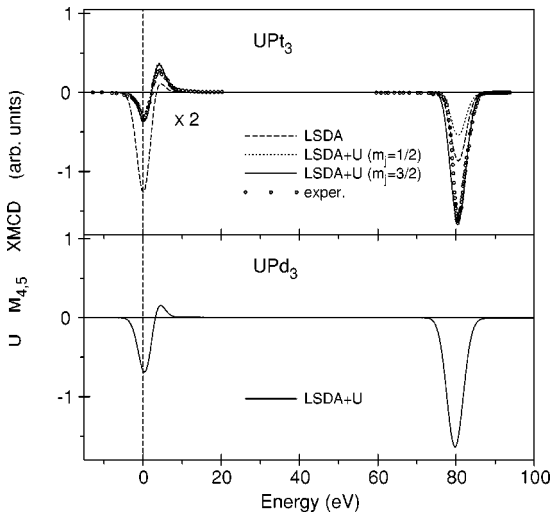

FIG. 4. The XMCD spectra of UPt_3 and UPd_3 at the uranium $M_{4,5}$ edges calculated in the LSDA, LSDA+U(OP), and LSDA +U. Experimental spectra for UPt_3 (Ref. 9) (circles) were measured in a magnetic field of 5 T at 20 K. (U M_4 spectra are shifted by -95 eV to include them in the figure).

spectrum of U at the M_4 edge ($I=\mu^- - \mu^+$) can be roughly represented by $-[N^{5/2}_{3/2}+N^{5/2}_{5/2}]$ partial density of states.[12] In the second case, however, the dipole allowed transitions for $\lambda=+1$ are $-1/2\rightarrow+1/2$, $+1/2\rightarrow+3/2$, and $+3/2\rightarrow+5/2$ and for $\lambda=-1$ are $-1/2\rightarrow-3/2$ and $+3/2\rightarrow+1/2$. Therefore U M_4 XMCD spectrum can be roughly represented by $N^{5/2}_{1/2}-[N^{5/2}_{3/2}+N^{5/2}_{5/2}]$ partial density of states. One would expect therefore smaller intensity of dichroic signal at the M_4 edge for the second case in comparison with the first one due to the compensation between $N_{1/2}$ and $[N_{3/2}+N_{5/2}]$ partial density of states in the second case.

The $5f_{7/2}$ states are almost completely empty in all the uranium compounds. Therefore the XMCD spectrum of U at the M_5 edge can be roughly represented by the m_j projected partial density of states:[12] $[N^{7/2}_{-7/2}+N^{7/2}_{-5/2}]-[N^{7/2}_{7/2}+N^{7/2}_{5/2}]$. As a result, the shape of the M_5 XMCD spectrum consists of two peaks of opposite sign—a negative peak at lower energy and a positive peak at higher energy. As the separation of the peaks is smaller than the typical lifetime broadening, the peaks cancel each other to a large extent, thus leading to a rather small signal.

Although we neglect cross terms in the transition matrix elements and there is no full compensation between transitions with equal final states due to difference in the angular matrix elements, such a simple representation qualitatively reproduces all the peculiarities of the experimentally measured XMCD spectra in UPt_3. It gives a simple, slightly asymmetric negative peak at the M_4 edge and an *s*-shaped two peak structure at the M_5 edge (Fig. 3). It also correctly gives the dichroism at the M_4 edge of approximately one order of magnitude larger than at the M_5 one. The spectrum at the M_4 edge is very sensitive to the character of the occupied $5f_{5/2}$ states and has larger intensity for the solution with occupied $|\frac{5}{2},-\frac{3}{2}\rangle$ states.

Figure 4 shows the calculated XMCD spectra in the LSDA and LSDA+U approximations for UPt_3 together with the experimental data.[9] The intrinsic broadening mechanisms have been accounted for by folding the XMCD spectra with a Lorentzian of 3.2 and 3.4 eV for M_5 and M_4 spectra, respectively. The overall shapes of the calculated and experimental uranium $M_{4,5}$ XMCD spectra correspond well to each other. The major discrepancy between the calculated and experimental XMCD spectra is the size of the M_4 XMCD peak. The LSDA theory produces a much smaller intensity for the XMCD spectrum at the M_4 edge in comparison with the experiment and simultaneously gives a larger dichroic signal at M_5 edge. On the other hand, the LSDA+U produces excellent agreement in the shape and intensity of XMCD spectra both at the M_4 and M_5 edges for the solution with the $|\frac{5}{2},-\frac{3}{2}\rangle$ state occupation. The solution with $|\frac{5}{2},-\frac{1}{2}\rangle$ occupation produces a smaller intensity for the XMCD spectrum at the M_4 edge in comparison with the experiment. This observation is consistent with the total-energy calculations which show that the lowest-energy state has the solution with $|\frac{5}{2},-\frac{3}{2}\rangle$ states occupied.

The LSDA with $U_{\rm eff}=0$, the so-called orbital polarization approximation [LSDA+U(OP)], which describes the correlations between spin and orbital magnetic moment directions, gives a correct value of the XMCD spectrum at the U M_4 edge, but slightly overestimates the positive peak and underestimates the negative one at the M_5 edge (not shown).

Figure 4 shows also the XMCD spectra in UPd_3 calculated using the LSDA+U for the solution with occupied $|\frac{5}{2},-\frac{3}{2}\rangle$ states. The XMCD spectra of UPd_3 and UPt_3 are very similar, except, the positive peak at the M_5 edge is slightly less pronounced in UPd_3 than in UPt_3. Experimental measurements of XMCD spectra in UPd_3 are highly desired.

IV. URu_2Si_2

The heavy-fermion superconductor URu_2Si_2 has attracted continuous attention in the last decade for its unusual ground-state properties. URu_2Si_2 crystallizes in the body-centered tetragonal $ThCr_2Si_2$ structure with lattice constant $a=4.126$ Å and $c/a=2.319$. At $T_N=17.5$ K the system undergoes an antiferromagnetic phase transition which is accompanied by a sharp peak in the specific heat[39,40] and thermal expansion.[41] A second transition occurs at $T_c=1.2$ K and indicates the onset of superconductivity which coexists with the antiferromagnetic order. Neutron-scattering measurements[42,43] revealed a simple antiferromagnetic structure with a tiny ordered moment of $(0.04\pm0.01)\mu_B$/U atom, oriented along the c axis of the tetragonal crystal structure. The formation of an energy gap in the magnetic excitation spectrum is reflected by an exponential temperature dependence of the specific heat,[39,40] the thermal expansion,[41] and the nuclear-magnetic-resonance and nuclear-quadruple-resonance relaxation rates[44] in the ordered state. Electrical resistivity[45] and point-contact spectroscopy measurements[46] show a similar energy gap, indicating a strong scattering of the conduction electrons by the magnetic excitations. Magnetization measurements in high magnetic fields[47,48] show a suppression of the heavy-fermion state in three consecutive steps at 35.8, 37.3, and 39.4 T for fields along the easy axis $(B\|c)$. These transitions have been confirmed in high-field measurements of the magnetoresistance and Hall coefficient.[49]

There are several LSDA band-structure calculations of URu_2Si_2 in the literature.[50–53] A self-consistent calculation of electronic band structure for antiferromagnetically ordered URu_2Si_2 was performed using an all-electron fully relativistic spin-polarized linear augmented plane wave (LAPW) method by Yamagami and Hamada.[53] They obtained a magnetic moment at the uranium site with a tiny value of $0.09\mu_B$ due to cancellation between the spin and the orbital moments. The theoretically calculated frequencies as functions of the direction of applied magnetic field are in reasonable agreement with the dHvA frequencies measured by Ohkuni *et al.*[54]

The electronic band structure and the Fermi surface of paramagnetic URu_2Si_2 have been studied also with high-resolution angle-resolved photoemission spectroscopy in Ref. 55. It was found that Ru $4d$ bands form the main body of the valence band and exhibit a remarkable energy dispersion in qualitatively good agreement with the band-structure calculations. In addition to the dispersive Ru $4d$ bands, a less dispersive band was found near the Fermi level, which can be assigned to the U $5f$–Ru $4d$ hybridized band.

A. Band structure

Self-consistent LSDA calculations produce an antiferromagnetic ground state in URu_2Si_2 in agreement with the experimental observation.[41] The spin moment at the U site is obtained as $-0.04\mu_B$ and the orbital moment is $0.09\ \mu_B$. The total magnetic moment is, therefore, $0.05\mu_B$. This is in a good agreement with the magnetic moment of $0.04\ \mu_B$ observed by neutron-scattering measurements.[42,43] The fully relativistic spin-polarized LSDA energy band structure and total DOS of the antiferromagnetic URu_2Si_2 is shown in Fig. 5. Figure 6 shows the LSDA partial density of states of URu_2Si_2. Si $3s$ states are located mostly at the bottom of the valence band in the -11 to -8 eV energy interval. Si $2p$ states hybridize strongly with Ru $4d$, U $6d$, and U $5f$ valence states and occupy a wide energy range from -6.5 to 11 eV. There is an energy gap of around 0.5 eV between Si $3s$ and $3p$ states. Ru $4d$ states are situated below and above Fermi level in the -6.5 to 3.5 eV range. The Fermi level falls in the local minimum of Ru $4d$ states (Fig. 6). U $6d$

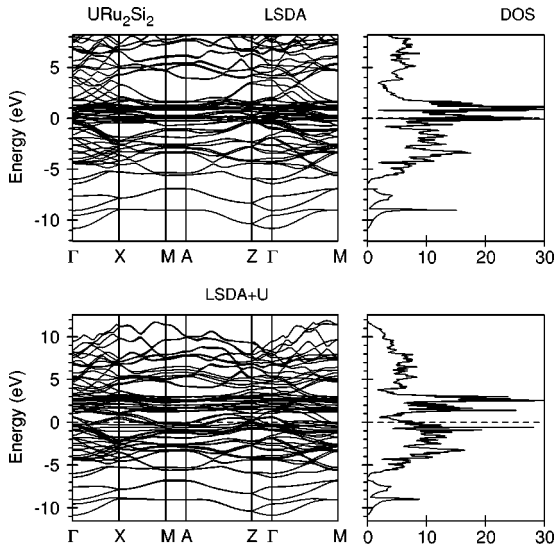

FIG. 5. The self-consistent fully relativistic, spin-polarized energy band structure and total DOS [in states/(unit cell eV)] of URu_2Si_2 calculated in the LSDA and LSDA$+U$.

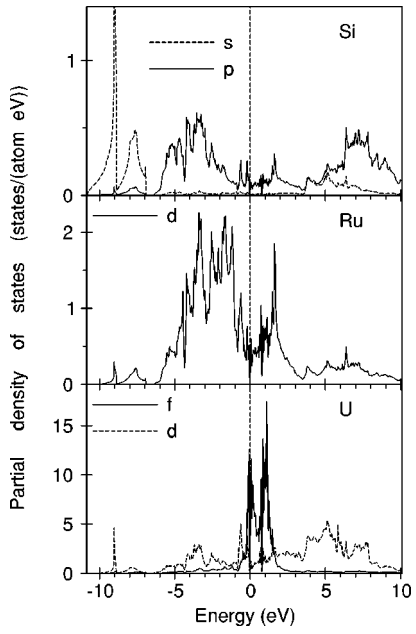

FIG. 6. The partial density of states in URu_2Si_2 calculated in the LSDA (the $6d$ partial DOS has been multiplied by factor of 3 for clarity).

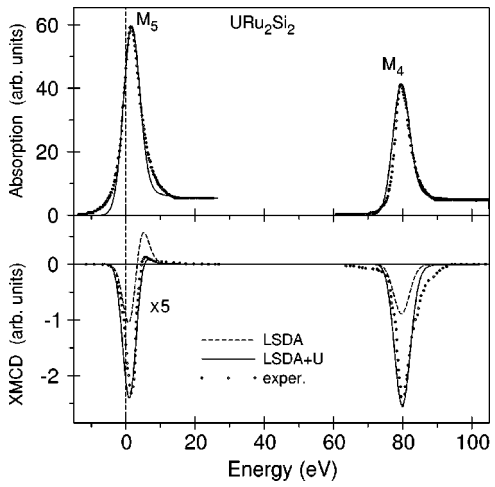

FIG. 7. Isotropic absorption and XMCD spectra of URu_2Si_2 at the uranium $M_{4,5}$ edges calculated in the LSDA (dashed lines) and LSDA+U (full lines). Experimental spectra (Ref. 11) (circles) were measured at 50 K and in a magnetic field of 5 T (U M_4 spectra are shifted by -95 eV to include them in the figure).

states are strongly hybridized with Ru $4d$ as well as Si $3p$ and even Si $3s$ states. A narrow peak of U $5f_{5/2}$ states is situated just at the Fermi level E_F. U $5f_{7/2}$ states are split off by strong SO coupling and form another narrow peak 1.2 eV above E_F. Because U $5f$ states are situated at the local minimum of Ru $4d$ states there is rather weak U $5f$—Ru $4d$ hybridization.

Figure. 5 also shows the band structure of URu_2Si_2 calculated in the LSDA+U with $U=2.0$ eV and $J=0.5$ eV. The Coulomb repulsion U_{eff} strongly influences the electronic structure of URu_2Si_2. The occupied on-site $5f$ energies are shifted downwards by $U_{\text{eff}}/2$ and the unoccupied levels are shifted upwards by this amount. As a result both the occupied and empty U $5f$ states move to a position with large Ru $4d$ DOS and the degree of U $5f$—Ru $4d$ hybridization increases going from the LSDA to the LSDA+U solution. In the Hartree-Fock-like LSDA+U solution with nonspherical correction to Coulomb matrix elements, three particular $5f_{5/2}$ states ($m_j=-5/2$, $m_j=-3/2$, and $m_j=-1/2$) are occupied, which leads to large spin ($-2.01\mu_B$) and orbital ($4.78\mu_B$) magnetic moments for the U atom. U $5f$ states just above the Fermi level are formed by the remaining $5f_{5/2}$ states whereas the peak of $5f_{7/2}$ states is pushed from its LSDA position above E_F by 2.8 eV.

B. XMCD spectra

Figure 7 shows the calculated x-ray isotropic absorption and XMCD spectra in the LSDA and LSDA+U for URu_2Si_2 together with the experimental data.[11] To calculate the x-ray isotropic absorption $M_{4,5}$ spectra we take into account the background intensity which appears due to transitions from occupied levels to the continuum of unoccupied levels.[56]

The theory produces a much smaller intensity of the XMCD spectrum at the M_4 edge in comparison with the experiment in the LSDA calculations. It also gives a larger positive peak and a two times smaller negative peak at the M_5 edge (Fig. 7). The LSDA+U with $J=2.0$ and $J=0.5$ eV and nonspherical corrections to Coulomb matrix elements[11] produces excellent agreement in shape and intensity for the XMCD spectra both at the M_4 and M_5 edges. This can be considered as evidence in favor of a picture of partly localized U $5f$ states in URu_2Si_2.

One should mention that the LSDA+U(OP) calculations ($U_{\text{eff}}=0$) underestimate the negative XMCD peak and overestimate the positive one at the M_5 edge (not shown). This approximation also slightly underestimates the XMCD signal at the M_4 edge.

V. UPd_2Al_3 AND UNi_2Al_3

The most recently discovered heavy-fermion superconductors UPd_2Al_3 and UNi_2Al_3 (Refs. 57 and 58) exhibit coexistence between superconductivity and a magnetic state with relatively large ordered magnetic moments. UPd_2Al_3 was found to exhibit a simple antiferromagnetic structure [wave vector $\vec{q}=(0,0,1/2)$] below $T_N\sim 14.5$ K and static magnetic moments of U lying in the basal plane.[59] The neutron-scattering data are consistent with an ordered magnetic moment $M_t\sim 0.85\mu_B$, reduced compared to the effective moment obtained from the high-temperature susceptibility, but exceeding by up to two orders of magnitude the small moments found, for example, in UPt_3. Hence, in contrast to UPt_3, a picture of local-moment magnetism seems to describe the magnetic state in UPd_2Al_3. Surprisingly, this large-moment magnetism was found to coexist with heavy-fermion superconductivity exhibiting the highest T_c reported to date for this class of materials.

The electronic structure and Fermi surface of the antiferromagnetic UPd_2Al_3 were calculated using the LSDA in Refs. 60–62. The calculated magnetic moment was in good agreement with experiment, as was the calculated magnetocrystalline anisotropy. The calculations reveal the importance of hybridization of the U $5f$ states with the valence states of Pd and Al even though this hybridization appears to be rather weak and to influence only a restricted energy interval in the U $5f$ bands. The calculated dHvA frequencies are found to be in good agreement with the experimental data. However, the observed heavy masses cannot be obtained within the LSDA.[62]

The measured (in Ref. 63) x-ray photoemission and bremsstrahlung isochromat spectra of UPd_2Al_3 are well reproduced by the LSDA calculated U $5f$ density of states. On the other hand, the resonance photoemission spectra of UPd_2Al_3 do not match the calculated U $5f$ DOS in shape or position, while the calculated Pd $4d$ DOS matches very well with the off-resonance spectrum.[64]

The superconducting and magnetic properties of UNi_2Al_3 are not so well documented compared to those of UPd_2Al_3 owing to the difficulties of preparing good single crystals.[10] UNi_2Al_3 undergoes transitions to antiferromagnetism at $T_N\sim 4.6$ K and to superconductivity at $T_C\sim 1.2$ K.[58] Muon spin rotation experiments[65] on polycrystalline UNi_2Al_3 showed evidence for antiferromagnetism with an ordered moment of the order of $0.1\mu_B$. Elastic neutron scattering from a single-

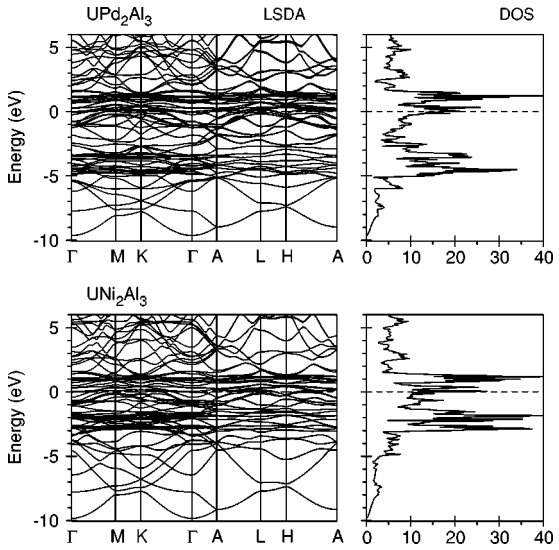

FIG. 8. The self-consistent fully relativistic, spin-polarized energy band structure and total DOS [in states/(unit cell eV)] of UPd_2Al_3 and UNi_2Al_3 calculated in the LSDA.

crystal sample of UNi_2Al_3 has revealed the onset of long-range magnetic order below $T_N = 4.6$ K.[66] The order is characterized by wave vector of the form $(\frac{1}{2} \pm \tau, 0, \frac{1}{2})$, with $\tau = 0.110 \pm 0.0003$, indicating an incommensurate magnetic structure within the basal plane, which is simply stacked antiferromagnetically along c to form the full three-dimensional magnetic structure. The maximum amplitude of the ordered moment is estimated to be $(0.21 \pm 0.10)\mu_B$.

A. Band structure

UPd_2Al_3 and UPd_2Al_3 crystallize in a rather simple hexagonal structure $P6/mmm$ (D^1_{6h}, $PrNi_2Al_3$-type structure) with lattice constant $a = 5.365$ Å, and $c/a = 4.186$ for UPd_2Al_3 and $a = 5.207$ Å and $c/a = 4.018$ for UNi_2Al_3.

The fully relativistic spin-polarized LSDA energy band structures and total DOS's of the antiferromagnetic UPd_2Al_3 and UNi_2Al_3 are shown in Fig. 8. The results of our band-structure calculations of UPd_2Al_3 are in good agreement with previous calculations of Sandratskii *et al.*[61] Al $3s$ states are located mostly at the bottom of the valence band in the -9.7 to -5 eV energy interval. Al $3p$ states occupy the wide energy range from -6 to 11 eV hybridized strongly with Pd $4d$, U $6d$, and U $5f$ valence states. Pd $4d$ states are almost fully occupied and situated below Fermi level in the -5 to -2.5 eV range. The magnetic moment at the Pd site, therefore, is extremely small. U $6d$ states are strongly hybridized with Pd $4d$ as well as Al $3p$ states. The characteristic feature of the LSDA band structure is a narrow peak of U $5f_{5/2}$ states situated just at the Fermi level E_F. U $5f_{7/2}$ states are split off by strong spin-orbit coupling and form another narrow peak 1.2 eV above E_F. Because Pd $4d$ states are located far below the Fermi level, there is a rather weak U $5f$—Pd $4d$ hybridization. We should mention, however, that this hybridization is of primary importance and influences greatly the form and width of the $5f$ peaks (the analysis of the hybridization effects in UPd_2Al_3 are presented in Ref. 61).

In agreement with experiment[59] we found the basal plane of the hexagonal structure to be the plane of easy magnetization in UPd_2Al_3. The magnetic structures with magnetic moments lying in the xy plane possess lower energy than those with atomic moments along the z axis. A rotation of the magnetic moment within the xy plane does not noticeably change the energy of the configuration as well as the value of the spin and orbital magnetic moments.

Our calculations, unfortunately, yield for the total energy of the in-plane ferromagnetic structure a slightly lower value than for the energy of the corresponding antiferromagnetic structure, although the difference of the total energy of the ferromagnetic and antiferromagnetic in-plane solutions is very small, about 9 meV per formula unit, and is close to the accuracy limit of our LMTO-LSDA calculations. This disagrees with experiment, which shows the ground-state magnetic structure to be antiferromagnetic.[59] The same results were obtained by Sandratskii *et al.* in Ref. 61.

The energy band structures of UNi_2Al_3 and UPd_2Al_3 are very similar (Fig. 8). The major difference is in the energy location and width of the transition-metal bands. Due to less spatial expansion of Ni $3d$ wave functions compared to Pd $4d$ wave functions the Ni $3d$ energy band is 1.5 times narrower than the corresponding $4d$ band in UPd_2Al_3. The Ni $3d$ energy band is situated in the -3 to -1.2 eV energy interval. Due to a shift of the Ni $3d$ band toward the Fermi level, the U $5f$—Ni $3d$ hybridization in UNi_2Al_3 is increased in comparison with the U $5f$—Pd $4d$ hybridization in UPd_2Al_3. A stronger interaction between $5f$ and conduction electrons when replacing Pd by Ni is manifested in a shift toward higher temperatures of the maxima of both the resistivity and the susceptibility together with the decrease of the magnetic ordering temperature T_N, the superconductivity temperature T_C, the antiferromagnetic moment, and the smaller entropy change at T_N.[10]

Figure 9 shows m_j projected $5f_{5/2}$ density of states in UPd_2Al_3 calculated in the LSDA and LSDA$+U$. We performed two LSDA$+U$ band-structure calculations. In the first calculation we used $U = J = 0.5$ eV, which gives $U_{\text{eff}} = 0$ [the so-called LSDA$+U$(OP)]. In the second one $U = 2.0$ eV and $J = 0.5$ eV. The LSDA approximation places the $5f_{5/2}$ density of states in close vicinity of the Fermi level at -0.5 to 0.5 eV with strong hybridization between states with different m_j. The Coulomb repulsion U_{eff} strongly influences the electronic structure of UPd_2Al_3 and UNi_2Al_3. In the Hartree-Fock like LSDA$+U$ solution with nonspherical corrections to Coulomb matrix elements, three particular $5f_{5/2}$ states ($m_j = -5/2$, $m_j = -3/2$, and $m_j = -1/2$) are almost completely occupied producing the $5f^3$ configuration for U in UPd_2Al_3 and UNi_2Al_3.

Table I lists the calculated spin M_s, orbital M_l, and total M_t magnetic moments (in μ_B) as well as the ratio M_l/M_s in UPd_2Al_3 and UNi_2Al_3. Our LSDA results are in good agreement with previous LSDA calculations.[61] Surprisingly, LSDA calculations produce the *total* magnetic moments in

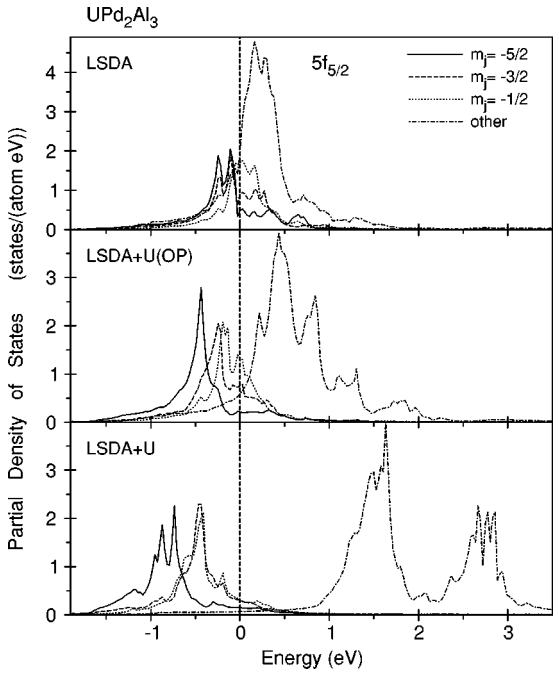

FIG. 9. The partial $5f_{5/2}$ density of states (in states/atom eV) in UPd_2Al_3.

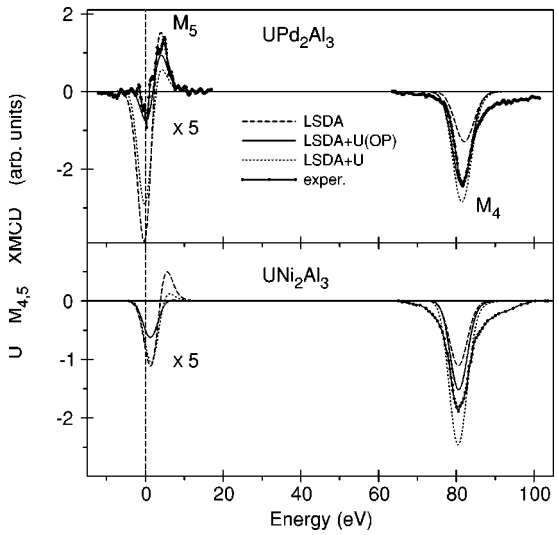

FIG. 10. The XMCD spectra of UPd_2Al_3 and UNi_2Al_3 at the uranium $M_{4,5}$ edges calculated in LSDA and LSDA+U. Experimental spectra for UPd_2Al_3 (Ref. 11) were measured in a magnetic field of 5 T and 35 K. The experimental data for the U M_4 XMCD spectrum of UNi_2Al_3 is from Ref. 10. (U M_4 spectra are shifted by -95 eV to include them in the figure).

UPd_2Al_3 and UNi_2Al_3 in good agreement with the experimental data. On the other hand, the LSDA calculations strongly underestimate the ratio M_l/M_s (especially in UNi_2Al_3) due to the underestimation of the orbital moment by LSDA-based computational methods. The ratio M_l/M_s in the LSDA+U(OP) calculations is in reasonable agreement with the experimental data for both compounds.

B. XMCD spectra

Figure 10 shows the calculated XMCD spectra in the LSDA, LSDA+U(OP), and LSDA+U for UPd_2Al_3 together with the corresponding experimental data.[11] The overall shapes of the calculated and experimental uranium $M_{4,5}$ XMCD spectra correspond well to each other. The major discrepancy between the calculated and experimental XMCD spectra is the size of the M_4 XMCD peak. The LSDA theory produces much smaller intensity for the XMCD spectrum at the M_4 edge in comparison with experiment and simultaneously strongly overestimates the negative peak at the M_5 edge. On the other hand, the LSDA+U(OP) produces an excellent agreement in the shape and intensity of the XMCD spectra both at the M_4 and M_5 edges. The LSDA+U calculations with $U=2.0$ eV slightly overestimate the intensity of the dichroic signal at the M_4 edge and produce a larger negative peak and smaller positive one at the M_5 edge.

Figure 10 shows also the XMCD spectra for UNi_2Al_3. The experimental data exist only for the M_4 edge in this compound.[10] For the LSDA calculations the theory produces a smaller intensity of the XMCD spectrum at the M_4 edge in comparison with the experiment. On the other hand, the intensity of the experimentally measured M_4 XMCD spectrum is in between the results obtained by LSDA+U(OP) and LSDA+U.

TABLE I. The experimental and calculated spin M_s, orbital M_l, and total M_t magnetic moments at uranium site (in μ_B) of UPd_2Al_3 and UNi_2Al_3. The magnetic moments calculated for easy magnetic axes, namely, hexagonal plane in UPd_2Al_3 and c axis in UNi_2Al_3.

Compound	Method	M_s	M_l	M_t	$-M_l/M_s$
UPd_2Al_3	LSDA	−1.38	2.22	0.84	1.61
	LSDA (Ref. 61)	−1.62	2.49	0.87	1.54
	LSDA+U(OP)	−1.59	3.73	2.14	2.34
	LSDA+U	−1.92	4.61	2.69	2.40
	Expt. (Ref. 59)			0.85	
	Expt. (Ref. 10)				2.01
	Expt.[11]				1.91
UNi_2Al_3	LSDA	−0.47	0.54	0.07	1.15
	LSDA+U(OP)	−1.22	2.90	1.68	2.38
	LSDA+U	−1.74	4.46	2.72	2.56
	Expt. (Ref. 59)			0.2	
	Expt. (Ref. 10)				2.49

VI. UBe_{13}

The system UBe_{13} was the first U-based heavy-fermion superconductor discovered[67] and, similar to UPt_3, it shows peculiar properties, pointing to an unconventional superconducting order parameter. UBe_{13} is certainly the most anomalous of the heavy-fermion superconductors.

The specific heat in UBe_{13} is very weakly dependent upon magnetic field and highly sensitive to pressure.[68] The low-temperature value of the electronic specific-heat coefficient γ is of the order of 1000 mJ mol^{-1} K^{-2}, corresponding to an

effective mass of several hundred free-electron masses. The magnetic susceptibility is weakly pressure dependent in comparison with the specific heat and under pressure has a completely different temperature dependence.[69] Doping on the U sublattice which drives away the specific-heat anomaly leaves the low-temperature susceptibility essentially unchanged. The magnetization is linear in fields up to 20 T.[68]

The dynamic magnetic susceptibility reveals no significant structure on the scale of 1 meV, as is evidenced in C/T and instead shows a broad ''quasielastic'' response on the scale of 15 meV as evidenced in both neutron scattering and Raman spectra. Concomitant with the peak in χ'' is a Schottky anomaly in the specific heat, suggesting that the 15 meV peak represents highly damped crystal-field levels for which further evidence appears in the nuclear-magnetic relaxation of the ^{9}Be sites. This dynamic susceptibility peak integrates to give 80% of the static susceptibility up to the experimental cutoff. This places a stringent bound on any hypothetical moment-carrying state in the low-frequency region; given a 10 K Kondo scale to explain the residual susceptibility the effective squared moment must be less than $0.25\mu_B$, which would appear to rule out an interpretation in terms of a $5f^3\Gamma_6$ ground state.[68]

There are several different interpretations of these experimental data in literature. Miranda and co-workers suggested the non-Fermi-liquid (NFL) behavior of UBe_{13} could be driven by disorder.[70] Cox proposed, based on symmetry grounds, that the NFL behavior can be explained by the two-channel Kondo model description.[71] More recently, Anders *et al.* tackled the problem for the corresponding lattice model.[72] They also performed a calculation of the optical properties within such a two-channel Anderson lattice model for which the suppression of the low-frequency Drude component and the development of a mid-infrared absorption in the excitation spectrum at low temperatures have been suggested.[72]

One framework for describing the low-temperature properties of UBe_{13} characterizes the material's behavior in terms of its energy scales. Whereas common metals may be characterized by a single energy scale (the Fermi energy), UBe_{13} appears to require several. One may consider four energy scales:[68] a crystal-field splitting of 150–189 K, a Kondo temperature of about 25 K, a spin-fluctuation temperature of about 2 K, and the superconducting transition temperature of about 0.8 K.

The energy band structure and Fermi surface of UBe_{13} have been investigated in Refs. 73–76 in a frame of the LSDA. It was shown[76] that the hybridization between the U $5f$ states and the Be $2p$ states occurs in the vicinity of the Fermi level. The sheets of the Fermi surface are all small in size and closed in topology. The cyclotron effective mass calculated for the dHvA branches in the three symmetry directions varies from $1.08m_0$ to $4.18m_0$. The theoretical electronic specific-heat coefficient γ_{band}^{LDA} is 13.0 mJ/K^2 mol.[76] The theoretical results for the electronic specific-heat coefficient are much less than the experimental ones, suggesting a large enhancement due to many-body effects. This disagreement between theory and experiment might be ascribed to the enhancements due to the electron correlations and/or the electron-phonon interaction which the LSDA fails to take into account.

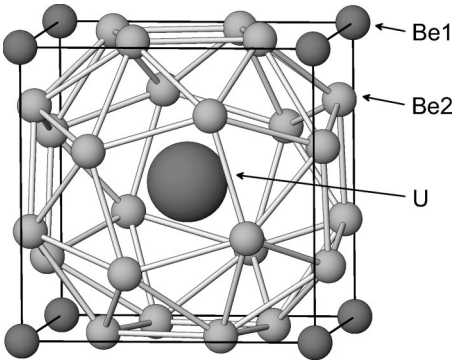

FIG. 11. Crystal structure of UBe_{13}.

A. Band structure

UBe_{13} crystallizes in the $NaZn_{13}$-type fcc structure with the space group O_h^6-$Fm3c$ (No 226) and contains 28 atoms per unit cell. There are two distinct Be sites, Be_1 and Be_2, with the 24 Be_2 sites having a very low site symmetry (only a mirror plane). The U atoms are surrounded by cages of 24 Be_2 atoms (Fig. 11) at the distance of 3.02 Å. Eight Be_1 atoms are separated from the U atom by 4.443 Å. This ensures that the U atoms are widely separated. The U atoms form a simple cubic sublattice with a large U-U nearest-neighbor distance of $a/2=5.13$ Å, which guarantees that the f-f overlap is negligible. Therefore, all broadening of the U $5f$ states into bands results entirely from hybridization with the conduction bands, rather than partially from direct f-f overlap, as occurs in many U compounds.

Self-consistent LSDA calculations produce a nonmagnetic ground state in UBe_{13}. To calculate the electronic structure and XMCD spectra of UBe_{13} in the LSDA, the term $2\mu_B\vec{B}\cdot\vec{s}$ which couples the spin of an electron to the external magnetic field was added to the Hamiltonian at the variational step. The fully relativistic spin-polarized LSDA energy band structure and total DOS of UBe_{13} is shown in Fig. 12 calculated in an external magnetic field of 20 T. The occupied part of the valence band is formed predominantly by Be $2s$ and $2p$ states. U $5f_{5/2}$ states are situated just at the Fermi level 1.0 eV above the top of Be $2p$ states. U $5f_{7/2}$ states are split off by strong SO coupling and form another narrow peak 1 eV above E_F. Be $2s$ states are located mostly at the bottom of the valence band. Be $2p$ states are strongly hybridized with U $6d$ states in the -6 to -1 eV energy interval. On the other hand, there is quite large U $5f$–Be $2p$ hybridization in vicinity of the Fermi level in the -0.6 to 1.4 eV energy range. Although every individual Be atom produces a quite small $2p$ partial density of states, due to the large number of Be atoms they sum up to a $2p$ DOS comparable in intensity with the U $5f$ DOS (Fig. 12).

Figure 12 also shows the band structure of UBe_{13} calculated in the LSDA+U with $U=2.0$ eV and $J=0.5$ eV. Partially occupied U $5f_{5/2}$ states split due to the Coulomb repulsion and the LSDA+U calculations give a solution with

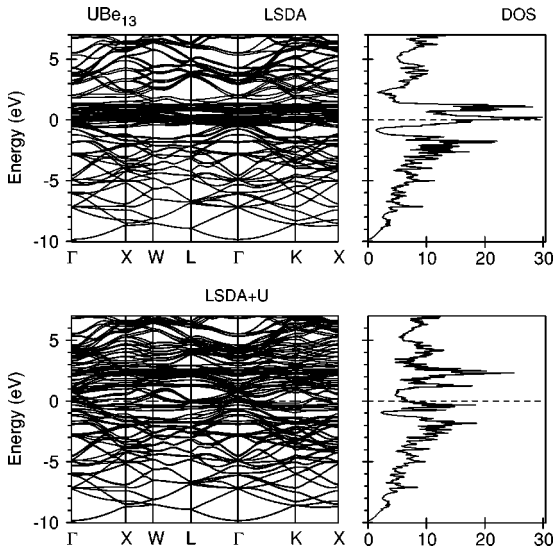

FIG. 12. The energy band structure and total density of states (in states/unit cell eV) in UBe_{13} calculated in the LSDA and LSDA $+U$.

three localized $5f$ electrons. These localized $5f$ states form a rather narrow peak at 0.6 eV below E_F. U $5f$ states just above the Fermi level are formed by the remaining $5f_{5/2}$ states whereas the peak of $5f_{7/2}$ states is pushed from its LSDA position at 1.2 eV above E_F to 2.2 eV.

Figure 13 shows m_j projected $5f_{5/2}$ and total $5f_{7/2}$ density of states in UBe_{13} calculated in the LSDA and LSDA$+U$. We performed two LSDA$+U$ band-structure calculations both with $U=2.0$ eV and $J=0.5$ eV. In the first calculation we used the LSDA$+U$ method with nonspherical corrections to the Coulomb matrix elements.[18] The effect of a less asymmetric density of localized $5f$ electrons can be simulated by replacing the matrix elements $U_{mmm'm'}$ and $J_{mm'm'm}$ by averaged Coulomb U and exchange J integrals, respectively, and setting all other matrix elements to zero.[18] In the nonrelativistic limit this would correspond, except for the approximation to the double counting term, to the original version of the LSDA$+U$ method proposed in Ref. 77. In this case all unoccupied U $5f$ electrons independent of their angular momentum experience the same Coulomb repulsion as the localized ones. In the Hartree-Fock-like LSDA$+U$ solution with nonspherical corrections to the Coulomb matrix elements three particular $5f_{5/2}$ states ($m_j=-5/2$, $m_j=-3/2$, and $m_j=-1/2$) are occupied which leads to (i) large spin ($-1.95\mu_B$) and orbital ($4.47\mu_B$) magnetic moments of the U atom and (ii) strongly anisotropic Coulomb interaction of the remaining $5f$ electrons with the occupied ones. In the calculations using the LSDA$+U$ method with spherically averaged U and J an unoccupied U $5f$ electron state feels a much more isotropic repulsive potential and is situated closer to the Fermi energy. This gives smaller magnetic moments (spin moment is equal to $-1.82\mu_B$ and orbital moment $4.08\mu_B$) in comparison with the nonspherical solution. The $5f_{5/2}$ states with $m_j=-1/2$ became partly empty for the calculations with spherically averaged U and J and the main peak of $N_{-1/2}$ DOS is situated just above the Fermi level (Fig. 13).

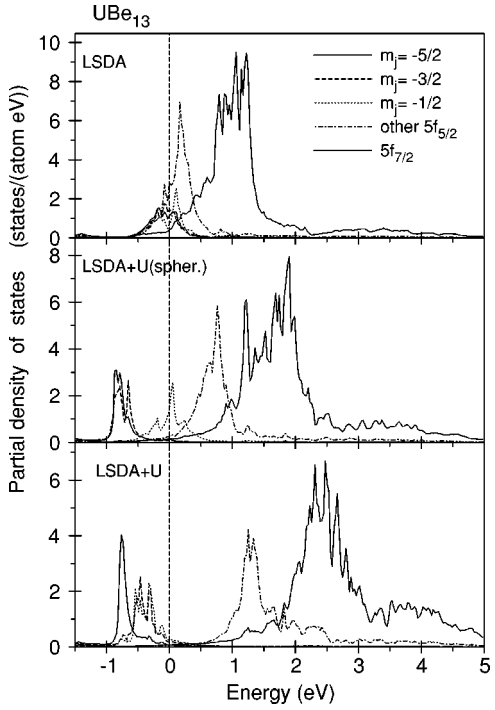

FIG. 13. The m_j projected $5f_{5/2}$ and total $5f_{5/2}$ density of states in UBe_{13} calculated in the LSDA and LSDA$+U$.

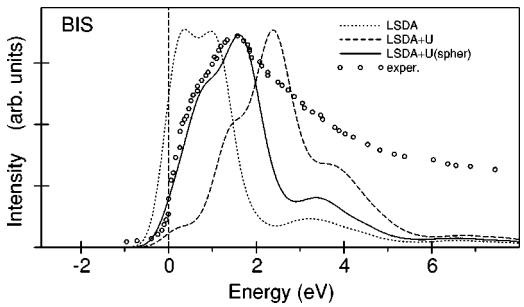

FIG. 14. Comparison of the calculated U partial $5f$ DOS in the LSDA (dotted line) and LSDA$+U$ with the experimental BIS spectrum (circles) of UBe_{13} (Ref. 78). Dashed line presents DOS calculated with nonspherical correction to Coulomb matrix elements whereas full line is calculated with averaged U and J.

The three calculations presented in Fig. 13 produce rather different energy locations for the empty $5f$ states. The principal question of the energy position of the empty $5f$ states is usually answered by bremsstrahlung isochromat spectroscopy (BIS) measurements. Figure 14 shows the experimental BIS spectrum of UBe_{13} (Ref. 78) compared with the calculated energy distribution for the unoccupied partial U $5f$ density of states in the LSDA and LSDA$+U$. The LSDA places empty $5f$ states too close to the Fermi level (Fig. 14). The LSDA$+U$ calculations with nonspherical solution place the maximum of empty $5f$ states more than 1 eV higher than the experiment. The LSDA$+U$ calculations with spherically averaged U and J give the correct position of empty $5f$ states within the experimental resolution (Fig. 14). The main peak

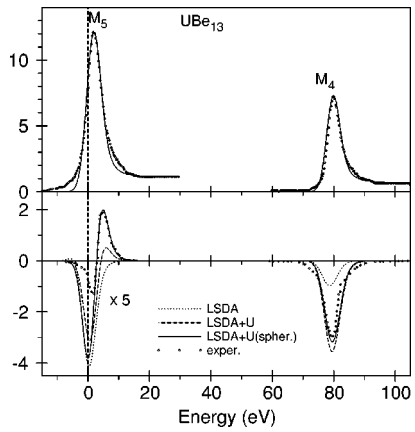

FIG. 15. Isotropic absorption and XMCD spectra of UBe_{13} at the uranium $M_{4,5}$ edges calculated in the LSDA (dotted lines) and LSDA+U. The dashed line presents XMCD spectra calculated with nonspherical corrections to Coulomb matrix elements whereas the full line results are calculated with averaged U and J. Experimental spectra (Ref. 9) (circles) were measured at 12 K and in a magnetic field of 5 T (the U M_4 spectrum is shifted by -95 eV to include it in the figure).

in the BIS spectrum is derived from the U $5f_{7/2}$ states, while the low-energy shoulder split off from the main peak is from the $5f_{5/2}$ states.

B. XMCD spectra

Figure 15 shows the UBe_{13} x-ray isotropic absorption and XMCD spectra calculated in the LSDA and LSDA+U together with the experimental data.[9] The LSDA calculations produce much smaller intensity of the XMCD spectrum at the M_4 edge in comparison with the experiment and simultaneously give larger dichroic signal for the negative peak and do not produce the positive shoulder at the M_5 edge (Fig. 15). On the other hand, the LSDA+U calculations improve the agreement between the theory and the experiment in the shape and intensity of XMCD spectra both at the M_4 and M_5 edges. The LSDA+U method with nonspherical corrections to the Coulomb matrix elements slightly overestimates the dichroic signal at the M_4 edge, underestimates the intensity of the positive peak, and strongly overestimates the negative peak at the M_5 edge. The LSDA+U calculations with averaged U and J give a correct value of the positive peak at the M_5 edge and the negative peak at the M_4 one but still overestimate the intensity of the negative peak at the M_5 edge.

UBe_{13} is unlike the other heavy-fermion compounds, in that the better description of its XMCD and BIS spectra requires spherically averaged U and J values. The physical reason for this is not clear, however there are some indications from the calculations. Comparing the orbital resolved $5f_{5/2}$ DOS's shown in Fig. 13 one can see that in the LSDA+U solution with nonspherical corrections to the Coulomb matrix elements three particular $5f_{5/2}$ states ($m_j=-5/2$, $m_j=-3/2$, and $m_j=-1/2$) are fully occupied, which leads to a pure $5f^3$ configuration. The calculations using the spherically averaged U and J values give a solution with partly empty $m_j=-1/2$ states with the main peak of the $N_{-1/2}$ DOS very close to the Fermi level (Fig. 13). This is the typical situation for a system with mixed valence.[79,80] One should mention that the LSDA+U method which combines LSDA with a basically static, i.e., Hartree-Fock-like, mean-field approximation for a multiband Anderson lattice model does not contain true many-body physics and cannot treat systems with mixed valence properly. The evaluation of the electronic structure of UBe_{13} needs further theoretical investigations.

VII. SUMMARY

We have studied by means of an *ab initio* fully relativistic spin-polarized Dirac LMTO method the electronic structure and the x-ray magnetic circular dichroism in UFe_2, UXAl (X=Co, Rh, and Pt), and heavy-fermion compounds UPt_3, URu_2Si_2, UPd_2Al_3, UNi_2Al_3, and UBe_{13}.

The LSDA calculations fail to produce the correct value of the orbital moment in most uranium compounds because in LSDA the Kohn-Sham equation is described by a local potential including the spin-dependent electron density but neglecting the electric current, which describes M_l. The LSDA+U improves greatly the agreement between the theory and the experiment in the description of the magnetic moments in UFe_2 and UXAl (X=Co, Rh, and Pt). The very small value of U magnetic moments in UPt_3, UPd_3, and UBe_{13} have not been produced by any kind of approximation, which emphasizes the importance of subtle many-body effects responsible for the magnetic-moment formation in these compounds. These findings illustrate that not everything about the electronic structure of heavy-fermion compounds can be explained with the approximations considered.

The overall shapes of the calculated and experimental uranium $M_{4,5}$ XMCD spectra correspond well to each other. The major discrepancy between the calculated and experimental XMCD spectra is the size of the M_4 XMCD peak. The LSDA theory produces usually much smaller intensity for the XMCD spectrum at the M_4 edge in comparison with the experiment and simultaneously gives inappropriate dichroic signal strength at the M_5 edge. It fails to produce a correct intensity of dichroic signal at the M_4 edge even in UFe_2 which is widely believed to have itinerant $5f$ electrons. As the integrated XMCD signal is proportional to the orbital moment this discrepancy could be related rather to an underestimation of the orbital moment by LSDA-based computational methods rather than to a failure in the description of the energy band structure of the itinerant $5f$ systems. The LSDA+U gives much better agreement in the shape and intensity of the XMCD spectra both at the M_4 and M_5 edges in uranium compounds.

Concerning the best description of line shape and intensity of the XMCD spectra, the investigated metallic uranium compounds fall into two groups according to the type of the LSDA+U method used. The LSDA+U(OP) ($U_{\rm eff}=0$) better describes the XMCD spectra in UFe_2, UXAl (X=Co, Rh, and Pt), UPd_2Al_3, and UNi_2Al_3 compounds. But the XMCD spectra of UPt_3, URu_2Si_2, and UBe_{13} are better de-

scribed by the LSDA+U method with $U=2.0$ eV and $J=0.5$ eV. It might be concluded to some extent that the last three compounds have a larger degree of localization than the compounds from the first group.

ACKNOWLEDGMENTS

This work was carried out at the Ames Laboratory, which is operated for the U.S. Department of Energy by Iowa State University under Contract No. W-7405-82. This work was supported by the Director for Energy Research, Office of Basic Energy Sciences of the U.S. Department of Energy. V.N.A. and A.N.Y. would like to thank Professor P. Fulde for his interest in this work, for helpful discussions on novel problems of the strongly correlated systems, and for hospitality received during their stay at the Max-Planck-Institute in Dresden. V.N.A. gratefully acknowledges the hospitality at Ames Laboratory during his stay.

*Permanent address: Institute of Metal Physics, Vernadsky Street, 03142 Kiev, Ukraine. Email address: antonov@ameslab.gov; anton@imp.kiev.ua

[1] F.J. Steglich, J. Aaarts, C.D. Bredl, W. Lieke, D. Meschede, W. Franz, and H. Schäfer, Phys. Rev. Lett. **43**, 1892 (1979).

[2] P. Santini, R. Lemanski, and P. Erdoes, Adv. Phys. **48**, 537 (1999).

[3] W. Potzel, G.M. Kalvius, and J. Gal, in *Moessbauer Studies on Electronic Structure of Intermetallic Compounds: Handbook on the Physics and Chemistry of Rare Earths*, edited by G.H.L.K. A. Gschneidner, Jr., L. Eyring, and G.R. Choppin (Elsevier, Amsterdam, 1993), Vol. 17.

[4] P. Fulde, J. Keller, and G. Zwicknagl, in *Solid State Physics*, edited by H. Ehrenreich and D. Turnbull (Academic Press, San Diego, CA, 1988), Vol. 17.

[5] A. Amato, Rev. Mod. Phys. **69**, 1119 (1997).

[6] M.B. Maple, J. Alloys Compd. **303-304**, 1 (2000).

[7] R. Joynt and L. Taillefer, Rev. Mod. Phys. **74**, 235 (2002).

[8] M. Sigrist and K. Ueda, Rev. Mod. Phys. **63**, 239 (1991).

[9] P.D. de Reotier, A. Yaouanc, G. van der Laan, N. Kernavanois, J.P. Sanchez, J.L. Smith, A. Hiess, A. Huxley, and A. Rogalev, Phys. Rev. B **60**, 10 606 (1999).

[10] N. Kernavanois, J.X. Boucherle, P.D. de Reotier, F. Givord, E. Lelievre-Berna, E. Ressouche, A. Rogalev, J.P. Sanchez, N. Sato, and A. Yaouanc, J. Phys.: Condens. Matter **12**, 7857 (2000).

[11] A. Yaouanc, P.D. de Reotier, G. van der Laan, A. Hiess, J. Goulon, C. Neumann, P. Lejay, and N. Sato, Phys. Rev. B **58**, 8793 (1998).

[12] V.N. Antonov, B.N. Harmon, and A.N. Yaresko, this issue, Phys. Rev. B **68**, 214424 (2003).

[13] V.N. Antonov, B.N. Harmon, O. Andryushchenko, L. Bekenev, and A.N. Yaresko, preceding paper, Phys. Rev. B **68**, 214425 (2003).

[14] O.K. Andersen, Phys. Rev. B **12**, 3060 (1975).

[15] V.V. Nemoshkalenko, A.E. Krasovskii, V.N. Antonov, V.N. Antonov, U. Fleck, H. Wonn, and P. Ziesche, Phys. Status Solidi B **120**, 283 (1983).

[16] U. von Barth and L. Hedin, J. Phys. C **5**, 1629 (1972).

[17] P.E. Blöchl, O. Jepsen, and O.K. Andersen, Phys. Rev. B **49**, 16 223 (1994).

[18] A.N. Yaresko, V.N. Antonov, and P. Fulde, Phys. Rev. B **67**, 155103 (2003).

[19] G.R. Stewart, Z. Fisk, J.O. Willis, and J.L. Smith, Phys. Rev. Lett. **52**, 679 (1984).

[20] G. Stewart, Rev. Mod. Phys. **56**, 755 (1984).

[21] R. Albers, A.M. Boring, and N.E. Christensen, Phys. Rev. B **33**, 8116 (1986).

[22] M.R. Norman, R.C. Albers, A.M. Boring, and N.E. Christensen, Solid State Commun. **68**, 245 (1988).

[23] N. Kimura, R. Settai, Y. Onuki, H. Toshima, E. Yamamoto, K. Maezawa, H. Aoki, and H. Harima, J. Phys. Soc. Jpn. **64**, 3883 (1995).

[24] S.R. Julian, G.J. Teunissen, N. Dorion-Leyraund, A.D. Huxley, M.P. Ray, M.R. Norman, J. Floquet, and G.G. Lonzarich, *The Fermi Surface of UPt_3* (Cambridge, University Press, Cambridge, 2000).

[25] G. Zwicknagl, A.N. Yaresko, and P. Fulde, Phys. Rev. B **65**, 081103 (2002).

[26] L. Taillefer and G.G. Lonzarich, Phys. Rev. Lett. **60**, 1570 (1988).

[27] L. Taillefer, R. Newbury, G.G. Lonzarich, Z. Fisk, and J.L. Smith, J. Magn. Magn. Mater. **63-64**, 372 (1987).

[28] N. Kimura, T. Komatsubara, D. Aoki, Y. Onuki, Y. Haga, E. Yamamoto, H. Aoki, and H. Harima, J. Phys. Soc. Jpn. **67**, 2185 (1998).

[29] R.H. Heffner, D.W. Cooke, A.L. Giorgi, R.L. Hutson, M.E. Schillaci, H.D. Rempp, J.L. Smith, J.O. Willis, D.E. MacLaughlin, C. Boekema, R.L. Lichti, J. Oostens, and A.B. Denison, Phys. Rev. B **39**, 11 345 (1989).

[30] G. Aeppli, E. Bucher, A.I. Goldman, G. Shirane, C. Broholm, and J.K. Kjems, J. Magn. Magn. Mater. **76-77**, 385 (1988).

[31] S.M. Hayden, L. Taillefer, C. Vettier, and J. Flouquet, Phys. Rev. B **46**, 8675 (1992).

[32] B. Lussier, B. Ellman, and L. Taillefer, Phys. Rev. B **53**, 5145 (1996).

[33] E.D. Isaacs, P. Zschack, C.L. Broholm, C. Burns, G. Aeppli, A.P. Ramirez, T.T.M. Palstra, R.W. Erwin, N. Stcheli1, and E. Bucher, Phys. Rev. Lett. **75**, 1178 (1995).

[34] J.W. Allen, J.D. Denlinger, Y.X. Zhang, G.-H. Gweon, S.-H. Yang, S.-J. Oh, E.-J. Cho, W.P. Ellis, D.A. Gajewski, R. Chau, and M.B. Maple, Physica B **281-282**, 725 (2000).

[35] T. Ito, H. Kumigashira, S. Souma, T. Takahashi, Y. Tokiwa, Y. Haga, and Y. Onuki, Physica B **312-313**, 653 (2002).

[36] Y. Tokiwa, K. Sugiyama, T. Takeuchi, M. Nakashima, R. Settai, Y. Inada, Y. Haga, E. Yamamoto, K. Kindo, H. Harima, and Y. Onuki, J. Phys. Soc. Jpn. **70**, 1731 (2001).

[37] W.J.L. Buyers, A.F. Murray, T.M. Holden, and E.C. Svensson, Physica B & C **102**, 291 (1980).

[38] H. Harima, J. Magn. Magn. Mater. **226-230**, 83 (2001).

[39] T.T.M. Palstra, A.A. Menovsky, J. van der Berg, J. Dirkmaat, P.H. Kes, G.J. Nieuwenhuys, and J.A. Mydosh, Phys. Rev. Lett. **55**, 2727 (1985).

[40] W. Schlabitz, J. Baumann, B. Pollit, U. Rauchschwalbe, H.M. Mayer, U. Ahlheim, and C.D. Bredl, Z. Phys. B: Condens. Matter **62**, 171 (1986).

[41] A. de Visser, F.E. Kayzel, A.A. Menovsky, J.J.M. Franse, J.

van der Berg, and G.J. Nieuwenhuys, Phys. Rev. B **34**, 8168 (1986).
[42] C. Broholm, J.K. Kjems, W.J.L. Buyers, P. Matthews, T.T.M. Palstra, A.A. Menovsky, and J.A. Mydosh, Phys. Rev. Lett. **58**, 1467 (1987).
[43] C. Broholm, H. Lin, P.T. Matthews, T.E. Mason, W.J.L. Buyers, M.F. Collins, A.A. Menovsky, J.A. Mydosh, and J.K. Kjems, Phys. Rev. B **43**, 12 809 (1991).
[44] Y. Kohori, K. Matsuda, and T. Kohara, J. Phys. Soc. Jpn. **65**, 1083 (1996).
[45] S.A.M. Mentink, T.E. Mason, S. Suüllow, G.J. Nieuwenhuys, A.A. Menovsky, J. Mydosh, and J.A.A.J. Peerenboom, Phys. Rev. B **53**, R6014 (1996).
[46] K. Hasselbach, J.R. Kirtley, and P. Lejay, Phys. Rev. B **46**, 5826 (1992).
[47] A. de Visser, F.R. de Boer, A.A. Menovsky, and J.J.M. Franse, Solid State Commun. **64**, 527 (1987).
[48] K. Sugiyama, H. Fuke, K. Kindo, K. Shimohata, A.A. Menovsky, J.A. Mydosh, and M. Date, J. Phys. Soc. Jpn. **59**, 3331 (1990).
[49] K. Bakker, A. de Visser, A.A. Menovsky, and J.J.M. Franse, Physica B **186-188**, 720 (1993).
[50] M.R. Norman, T. Oguchi, and A.J. Freeman, Phys. Rev. B **38**, 11 193 (1988).
[51] L.M. Sandratskii and J. Kübler, Phys. Rev. B **50**, 9258 (1994).
[52] A. Continenza and P. Johansson, J. Magn. Magn. Mater. **140-144**, 1401 (1995).
[53] H. Yamagami and N. Hamada, Physica B **284-288**, 1295 (2000).
[54] H. Ohkuni, T. Ishida, Y. Inada, Y. Haga, E. Yamamoto, Y. Onuki, and S. Takahashi, J. Phys. Soc. Jpn. **66**, 945 (1997).
[55] T. Ito, H. Kumigashira, T. Takahashi, Y. Haga, E. Yamamoto, T. Honma, H. Ohkuni, and Y. Onuki, Physica B **281-282**, 727 (2000).
[56] F.K. Richtmyer, S.W. Barnes, and E. Ramberg, Phys. Rev. **46**, 843 (1934).
[57] C. Geibel, C. Schank, S. Thies, H. Kitazawa, C.D. Bredl, A. Booehm, M. Rau, A. Grauel, R. Caspary, R. Helfrich, U. Ahlheim, G. Weber, and F. Steglich, Z. Phys. B: Condens. Matter **84**, 1 (1991).
[58] C. Geibel, S. Thies, D. Kaczorowski, A. Mehner, A. Grauel, B. Seidel, U. Ahlheim, R. Helfrich, K. Petersen, C.D. Bredl, and F. Steglich, Z. Phys. B: Condens. Matter **83**, 305 (1991).
[59] A. Krimmel, P. Fischer, B. Roessli, H. Maletta, C. Geibel, C. Schank, A. Grauel, A. Loidl, and F. Steglich, Z. Phys. B: Condens. Matter **86**, 161 (1992).
[60] J. Sticht and J. Kübler, Z. Phys. B: Condens. Matter **87**, 299 (1992).
[61] L.M. Sandratskii, J. Kübler, P. Zahn, and I. Mertig, Phys. Rev. B **50**, 15 834 (1994).
[62] K. Knöpfle, A. Mavromaras, L.M. Sandratskii, and J. Kübler, J. Phys.: Condens. Matter **8**, 901 (1996).
[63] S. Fujimori, Y. Saito, M. Seki, K. Tamura, M. Mizuta, K. Yamaki, K. Sato, T. Okane, A. Tanaka, N. Sato, T. Komatsubara, Y. Tezuka, S. Shin, S. Suzuki, and S. Sato, J. Electron Spectrosc. Relat. Phenom. **101-103**, 439 (1999).
[64] T. Rjima, S. Sato, S. Suzuki, S. Fujimori, M. Yamada, N. Sato, Y. Onuki, T. Komatsubara, Y. Tezuka, S. Shin, and T. Ishii, J. Electron Spectrosc. Relat. Phenom. **78**, 147 (1996).
[65] A. Amato, C. Geibel, F.N. Gygax, R.H. Hefner, E. Knetsch, D.E. MacLaughlin, C. Schank, A. Schenck, F. Steglich, and M. Weber, Z. Phys. B: Condens. Matter **86**, 159 (1992).
[66] J.G. Lussier, M. Mao, A.A. Schröder, J. Garret, B.D. Gaulin, S.M. Shapiro, and W.J.L. Buyers, Phys. Rev. B **56**, 11 749 (1997).
[67] H.R. Ott, H. Rudigier, Z. Fisk, and J.L. Smith, Phys. Rev. Lett. **50**, 1595 (1983).
[68] D.L. Cox and A. Zawadowski, Adv. Phys. **47**, 599 (1998).
[69] M.W. McElfresh, M.B. Maple, J.O. Willis, D. Schiferl, J.L. Smith, Z. Fisk, and D.L. Cox, Phys. Rev. B **48**, 10 395 (1993).
[70] E. Miranda, V. Dobrosavljevic, and G. Kotliar, Phys. Rev. Lett. **78**, 290 (1997).
[71] D.L. Cox, Phys. Rev. Lett. **59**, 1240 (1987).
[72] F.B. Anders, M. Jarell, and D.L. Cox, Phys. Rev. Lett. **78**, 2000 (1997).
[73] K. Takegahara, H. Harima, and T. Kasuya, J. Phys. F: Met. Phys. **16**, 1691 (1986).
[74] M.R. Norman, W.E. Picket, H. Krakauer, and C.S. Wang, Phys. Rev. B **36**, 4058 (1987).
[75] K. Takegahara and H. Harima, Physica B **281-282**, 764 (2000).
[76] T. Maehira, A. Higashia, M. Higuchi, H. Yasuhara, and A. Hasegawa, Physica B **312-313**, 103 (2002).
[77] V.I. Anisimov, J. Zaanen, and O.K. Andersen, Phys. Rev. B **44**, 943 (1991).
[78] E. Wuilloud, Y. Baer, H.R. Ott, Z. Fisk, and J.L. Smith, Phys. Rev. B **29**, 5228 (1984).
[79] V.N. Antonov, B.N. Harmon, and A.N. Yaresko, Phys. Rev. B **66**, 165208 (2002).
[80] V.N. Antonov, A.N. Yaresko, and B.N. Harmon, Phys. Rev. B **66**, 165209 (2002).